 doi:10.20944/preprints201804.0335.v1

Communication

Mapping the Distribution of Particles in Hydrogel in Use for Nanoplasmonic Biosensors: A Comparison of Preparation Methods

Harald Ian Muri*, Linh Hoang, and Dag Roar Hjelme

Norwegian University of Science and Technology, Gunnerus Gate 1, 7012 Trondheim, Norway; linh.hoang@ntnu.no (L.H.) Department of Clinical and Molecular Medicine/Cellular and Molecular Imaging Core Facility; dag.hjelme@ntnu.no (D.R.H.) Department of Electronic Systems

* Correspondence: harald.muri@ntnu.no; Department of Electronic Systems; Tel.: +47-7341-2688

Abstract: The distribution of noble metal nanoparticles in hydrogels are influencing their nanoplasmonic response and signal used for biosensor purposes. By controlling the particle distribution, it is possible to obtain new nanoplasmonic features with new sensing modalities. Particle distributions can be characterized by using volume-imaging methods such as the focused ion beam-scanning electron microscope (FIB-SEM) and the serial block-face scanning electron microscopy (SBFSEM) techniques . Since the pore structure of hydrogels is contained by the water absorbed in the polymer network it may pose challenges for volume-imaging based on electron microscope techniques since the sample must be in a vacuum chamber. The structure of hydrogels can be conserved by choosing appropriate preparation methods, which also depends on the composition of the hydrogel used. In this paper, we have prepared low-weight percentage hydrogels, with and without gold nanorods (GNR) for conventional SEM imaging by using two different drying techniques; (1) the critical point drying (CPD) technique and (2) hexamethyldisilazane (HMDS) drying of hydrogels. A qualitative characterization of the GNR-hydrogels was carried out to study the GNRs positioned in the polymer network. The effect of the two different drying methods on the hydrogel morphology were also compared. The use of HMDS as an alternative to the CPD has several advantages involving less parametrical variables for drying, involving less effort, being cost-effective, and requires no equipment use. In addition, choosing an optimized sample preparation method for SEM with optimized imaging parameters is highly important for obtaining accurate information about materials that is not correlated to artifacts. Hence, the results obtained from the preparation methods and SEM imaging parameters in this paper are useful for developing methods for mapping the metal particle distributions in micro-hydrogels by using FIB-SEM and SBFSEM techniques.

Keywords: metal nanocomposite hydrogels; particle distribution; nanoplasmonic sensor; preparation methods; SEM imaging; volume imaging;

1. Introduction

The ability of a hydrogel to absorb large amounts of water without being dissolved have shown to be useful in a significant number of applications such as drug delivery systems, wound healing, protein purification, crystallization of minerals and sensor technologies [1–8]. The synthesis of hydrogels with properties as defined by the application in mind is possible by controlling the crosslinking density of the hydrogel, the polymer hydrophilicity, type of recognition entities as co-monomers in the polymer network, polymer ionicity, or polymer elasticity. The common functions of the polymer network consist of responding volumetrically to external stimuli such as pH [9–11], temperature [12–14], ionic strength [15–17], or receptor-analyte recombinations [18–21]. Some of these stimuli-responsive features of the hydrogel have shown to be very useful in controlling drug release [1] or to be useful for label-free and specific sensing of biomolecules [19,22]. Other properties of the gel-polymer network may also be of importance for the crystallization of minerals [4,23] or for the nucleation and growth

 doi:10.20944/preprints201804.0335.v1

of metal nanoparticles made by chemical reduction in the nano-fillers of the hydrogel matrix [24,25]. These hydrogels embedded with noble metal nanoparticles (NMNP) are fascinating materials often utilized for wound healing [26,27] but also impressive materials as nanoplasmonic systems [28,29]. NMNPs distributed in hydrogels exhibit intense optical scattering at specific light frequencies. This intense optical scattering phenomena arise from light interacting with confined collective oscillations of electron clouds in the NMNPs at a resonance frequency, also known as localized surface plasmon resonance (LSPR) [30–32]. LSPR of NMNPs may occur in the visible or infrared light-range and are frequently used in label-free biosensor applications due to the fast response times, high sensitivity, high selectivity and possibility for multianalyte sensing in complex mixtures [30,33–35]. LSPR of NMNP-hydrogels are dependent on the particle shape, size, the refractive index (RI) of the surrounding medium and the interparticle distances between the particles [36]. Coupling may occur between the resonant modes of the localized surface plasmons of NMNPs in close proximity to each other [37–40]. Hence, the scattering of NMNPs in a hydrogel may have a LSPR frequency for a random distribution of particles that is different from the LSPR frequency for an inhomogeneous particle distribution.

We have in earlier work developed proof-of-concepts fiber optic (FO) sensors based on using NMNPs immobilized in polyacrylamide hydrogels and based on combining LSPR and interferometric sensing modalities [41–43]. Here, the interferometric sensing modality detects the change in volume of a stimuli-responsive hydrogel whereas the LSPR sensing modality detects receptor-analyte recombinations on the NMNP surface. The dipole-dipole coupling and RI sensitivity of the LSPR in NMNPs may as well be utilized for detecting the change in volume of stimuli responsive hydrogels for significant swelling and deswelling.

The number density (ND) and the distribution of NMNPs in the hydrogel are influencing the LSPR response and the LSPR signal. For dipole-dipole coupling with $d \leq 5r$ (d is center-to-center interparticle distance and r is radius of particle) [44] it is possible to estimate the magnitude of this influence by computing the probability density of the interparticle distances from the nearest-neighbor distribution function (NNDF) [45–47]. By using results from [41] we can illustrate the computation of void NNDF of gold nanoparticles (GNP) (80 nm in diameter) embedded in hydrogel on an optical fiber (OF) end face as shown in Figure 1. The GNP-hydrogel on the OF end face responds to pH changes of the surrounding solution. A decreasing pH results in a deswelling of the GNP-hydrogel and that increases the ND. Thus, an increasing ND is decreasing the width of the NNDF and may decrease the linewidth of the LSPR signal for dipole-dipole coupled GNPs.

By using results from [41] it can be shown that significant LSPR shifts occurs for $d \leq 5r$ (see Figure 2). For GNPs distributed in a hydrogel, it is the NNDF of the average interparticle distance that is used for estimating the probability for dipole-dipole interactions to occur. Random distributed particles in a hydrogel may be explained from the results shown in Figure 1, but will deviate significantly from this model for an inhomogeneous particle distribution. Morphological characterization of inhomogeneous particle distributions in NMNP-hydrogels is thus necessary to study the origin of the observed optical properties.

Morphological characterizations of hydrogels are often performed by using scanning electron microscopy (SEM). Conventional SEM techniques requires the samples to be in a vacuum, which can pose challenges for conserving the native hydrated state of the hydrogel since its structure is contained by the water absorbed in the polymer network. To prevent a complete collapse of the hydrogel in the vacuum chamber it is possible to use different drying methods to conserve its pore structure. Pore structures of hydrogels can be conserved by using high or low temperature drying [48–50] or critical point drying (CPD) [49,51–53]. Different collapsing characteristics occurs for the different drying methods used which also depends on the composition of the hydrogel [49,54,55].

Preprints (www.preprints.org) | NOT PEER-REVIEWED | Posted: 26 April 2018 doi:10.20944/preprints201804.0335.v1

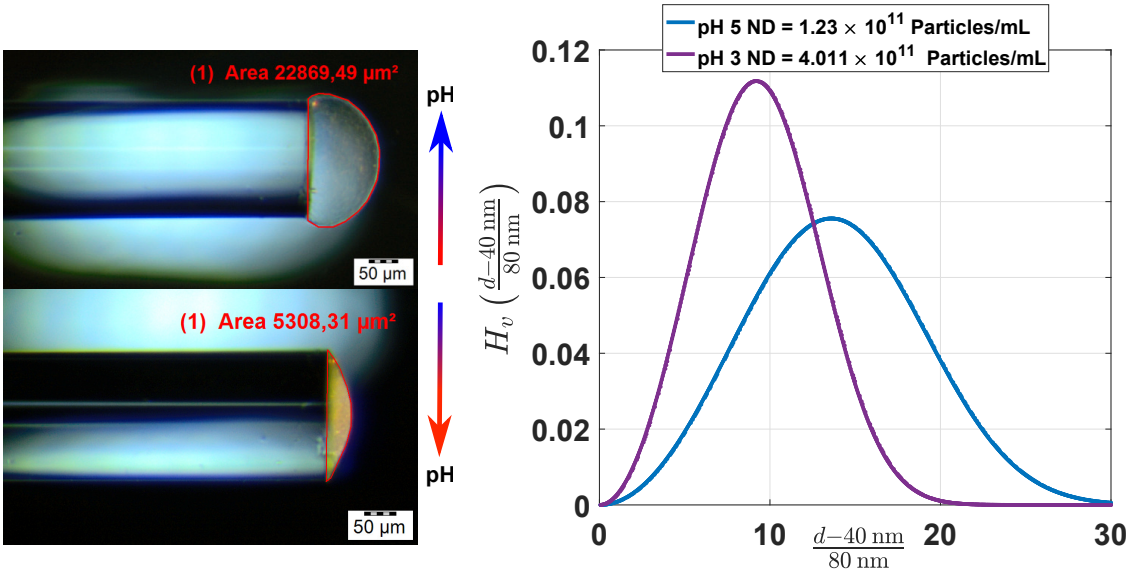

Figure 1. Computation of the NNDF of GNPs in hydrogel immobilized on an OF end face for different swelling equilibriums controlled with pH solutions. Decreasing pH increases the number density (ND) of GNPs since the hydrogel volume is decreasing. H_v is the NNDF, d is the center-to-center interparticle distance, 40 nm is the radius of the GNP and 80 nm is the diameter of the GNP. The optical microscope images and NNDF computations are from [41].

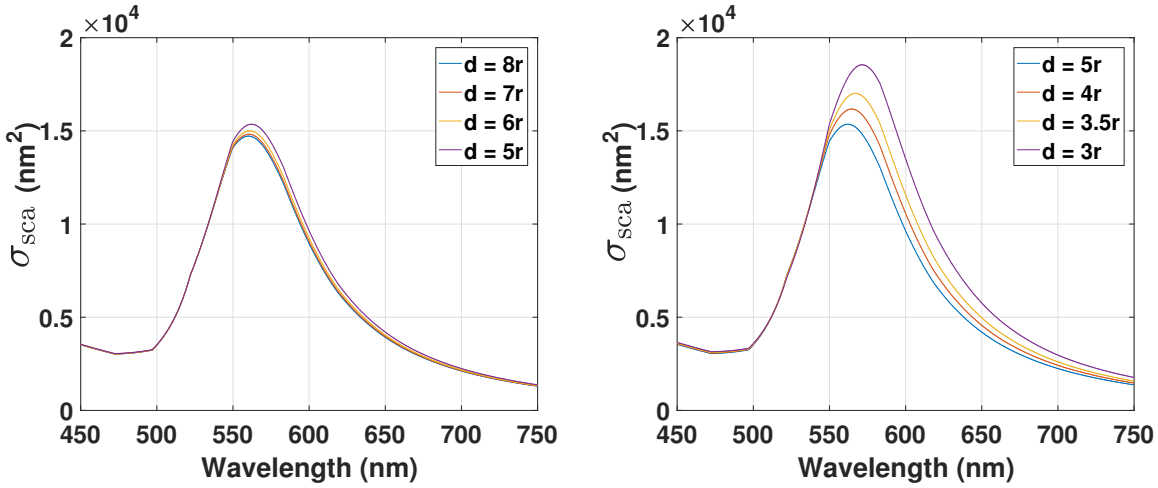

Figure 2. (**a**) Scattering cross-section (σ_{sca}) of GNP with 80 nm in diameter for $d \geq 5r$; (**b**) Scattering cross-section of GNP with 80 nm in diameter for $d \leq 5r$. The scattering cross-section is computed from results in [41].

By using specialized SEM techniques, such as cryoSEM or environmental-SEM, it is possible to characterize the morphology of hydrogels in their swelled state [51,56]. However, specialized SEM may have limit accessibility due to being a state-of-art technology. By using transmission electron microscopy, the high contrast of metal nanoparticles embedded in hydrogels can be observed, though, only a two dimensional particle distribution can be quantized [25,57]. Thus, to map the three

 doi:10.20944/preprints201804.0335.v1

dimensional distribution of particles in hydrogels with volume imaging methods, such as the focused ion beam-SEM technique (FIB-SEM) [58–60], conventional drying methods must be used.

In this paper we have studied the morphology of 10 wt% polyacrylamide (AAM-BIS) and poly(acrylamide-co-acrylic acid) (AAM-AAC-BIS) hydrogels, with and without gold nanorods (GNR), by using conventional SEM. The hydrogels were prepared for SEM by using two drying methods; (1) the critical point drying (CPD) technique and (2) the drying with hexamethyldisilazane (HMDS) solvent of hydrogels. The effect of the two different drying methods on the observed hydrogels morphology was compared. Furthermore, a qualitative characterization of the GNR-hydrogels was carried out to study the GNRs positioned in the polymer network, as well as the influence of GNR on the polymer network. The CPD technique is a common method for drying hydrogels to conserve the morphology in SEM imaging [49,51–53]. The air-drying with HMDS as an alternative to the CPD technique has its advantages; (1) less effort and fewer variables are involved; (2) it is cost-effective and (3) the method requires no equipment use. To the best of our knowledge, no morphological characterization of HMDS dried hydrogels have been performed with SEM. Hence, the comparison of the drying methods in this paper are useful for assessing HMDS as a drying method for hydrogels. Also, choosing an optimized sample preparation method for SEM with optimized imaging parameters is highly important for obtaining accurate information about materials that is not correlated to artifacts. The morphological results of the GNR-hydrogels obtained in this paper are thus useful as a first step in developing methods for mapping the distribution of particles in a micro-hydrogel by using volume imaging methods such as the FIB-SEM and the serial block-face scanning electron microscopy (SBFSEM) techniques [58–62].

2. Results and Discussion

2.1. Morphology of AAM-BIS Hydrogel With and Without GNRs

SEM images from CPD and HMDS dried hydrogels with GNRs in secondary electron (SE) and backscattered electron (BSE) mode are shown in Figure 3. Figure 3a and 3b shows hydrogels prepared with CPD, without and with GNRs in SE mode, respectively. The preparation methods may influence the pore structures as discussed in Section 2.3 [48,49]. In the SE mode SEM image of GNR-hydrogel in Figure 3b, no small-sized high contrast features can be observed. We may expect to observe high-density materials as high contrasts features such as from NMNPs in BSE mode at high electron beam voltages, since high-density materials have more substantial electron-backscattering intensities than low-density materials.

SEM images of HMDS dried hydrogels, with and without GNRs, are shown in Figure 3c and 3d in BSE mode, respectively. The pore sizes of the HMDS dried hydrogels are comparable to the SEM images of CPD hydrogels. This shows that using HMDS for drying hydrogels for SEM imaging may serve as a suitable alternative to the CPD technique. The drying with HMDS is a cost-effective substitution of the CPD technique that omits equipment use as well as it involves less parametrical variables in the drying. Pore sizes in HMDS dried hydrogels, with and without GNRs, are also comparable. The embedding of GNRs in the hydrogel have minor influence on the polymer network structure. In BSE mode, there are high contrast features along the edges of the pore structures in Figure 3d (indicated with white arrows), which could represent dense materials such as NMNP. The high contrast features are however similar for hydrogel, with and without GNRs, which makes the quantizing of the distribution of GNRs in the polymer network uncertain. The small-sized contrast features shown with white arrows in Figure 3d could be characterized as distributed GNRs, but may also be difficult to distinguish from artifacts associated to the sample preparation [63,64].

Figure 4 shows SEM images of CPD and HMDS dried hydrogels with GNRs at a higher magnification than the SEM-images in Figure 3. SEM image of GNR solution dried on carbon tape in Figure 4b is presented as a reference sample.

Preprints (www.preprints.org) | NOT PEER-REVIEWED | Posted: 26 April 2018 doi:10.20944/preprints201804.0335.v1

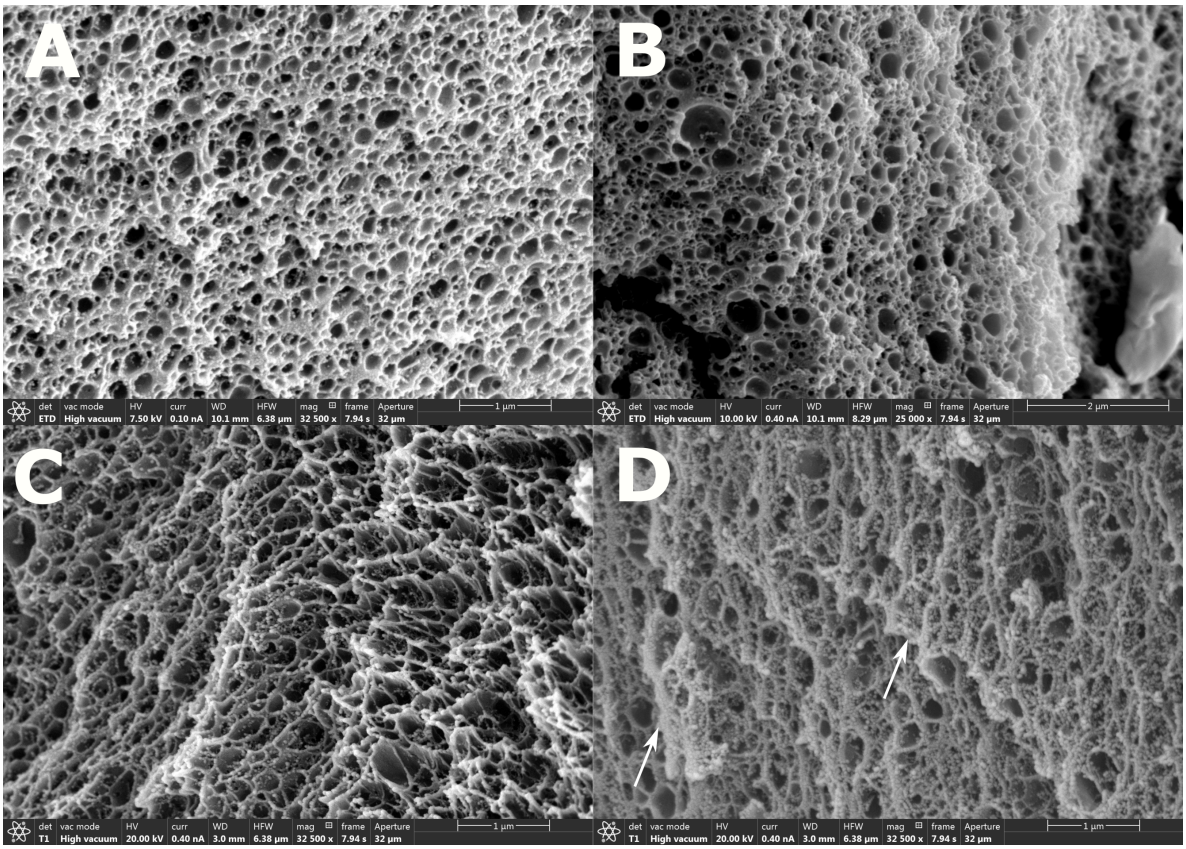

Figure 3. (**a**) SEM image of CPD AAM-BIS hydrogel without GNRs in SE mode; (**b**) SEM image of CPD AAM-BIS hydrogel with GNRs in SE mode; (**c**) SEM image of HMDS dried AAM-BIS hydrogel without GNP in BSE mode; (**d**) SEM image of HMDS dried AAM-BIS hydrogel with GNP in BSE mode. The white arrows clarifies the small-sized high contrast features observed that could indicate distributed GNRs.

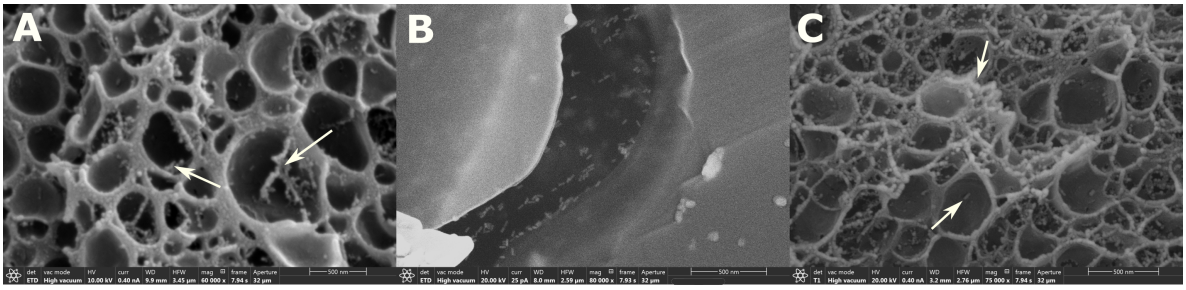

Figure 4. (**a**) SEM image of CPD AAM-BIS hydrogel with GNRs in SE mode; (**b**) Air-dried GNR solution on carbon tape in SE mode for comparison with SEM images of GNP-hydrogels; (**c**) SEM image of HMDS dried AAM-BIS hydrogel with GNP in BSE mode. The white arrows clarifies the small-sized high contrast features observed that could indicate distributed GNRs.

The GNRs in Figure 4b have length and width similar to the specifications received from the producer and is used for comparison to the small-sized high contrast features observable in Figure 4a and 4c (shown with white arrows). The pore structure of the hydrogel dried with CPD technique is similar to the HMDS dried GNR-hydrogel, which again demonstrates that drying with HMDS may serve as a useful alternative to the CPD technique. The BSE mode SEM image in Figure 4c shows few small-sized high contrast features (indicated with white arrows), which could indicate the presence of GNRs since they are denser than the polymer network. The dimension of the contrast features in

Preprints (www.preprints.org) | NOT PEER-REVIEWED | Posted: 26 April 2018 doi:10.20944/preprints201804.0335.v1

Figure 4a and 4c are comparable to the size of GNRs in Figure 4b, but difficult to quantize with respect to estimating the particle distributions. The contrast of NMNPs in gel-like samples may be improved by omitting the metal sample coating and by instead including highly conductive sample holders [65]. The detection of SE and BSE can also be combined to obtain density dependent contrasts that highlights the high densities areas in the image [66].

2.2. Morphology of AAM-AAC-BIS Hydrogel With and Without GNRs

SEM images of CPD and HMDS dried hydrogels, with and without GNRs, in SE and BSE mode are shown in Figure 5.

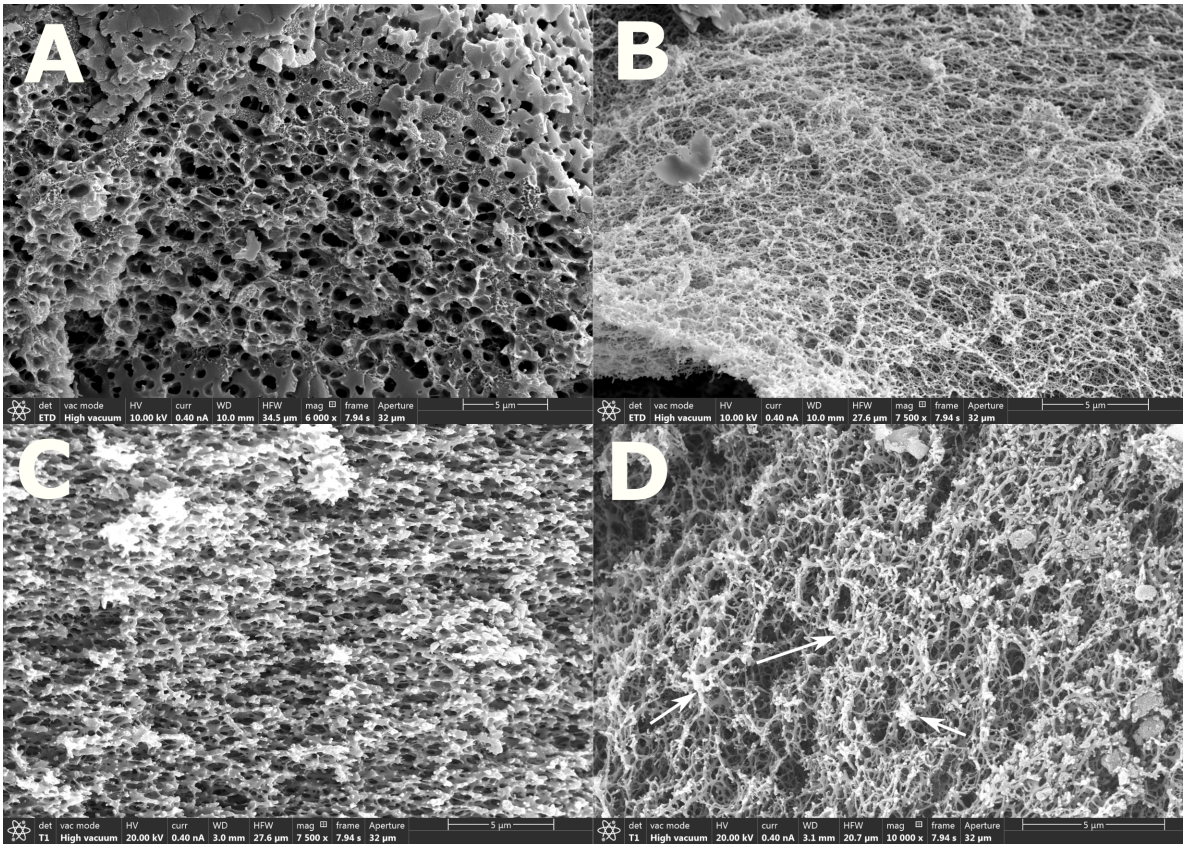

Figure 5. (**a**) SEM image of CPD AAM-AAC-BIS hydrogel without GNRs in SE mode; (**b**) SEM image of CPD AAM-AAC-BIS hydrogel with GNRs in SE mode; (**c**) SEM image of HMDS dried AAM-AAC-BIS hydrogel without GNP in BSE mode; (**d**) SEM image of HMDS dried AAM-AAC-BIS hydrogel with GNP in BSE mode. The white arrows clarifies the small-sized high contrast features observed that could indicate distributed GNRs.

Figure 5a and 5b shows CPD hydrogels without and with GNRs in SE mode, respectively. Some collapsing characteristics can be observed for the hydrogel without GNRs. The collapse could be a result of insufficient dehydration considering that the AAM-AAC-BIS hydrogels have 2/1 (AAC/AAM) molar ratio of hydrophilic anionic AAC co-monomers. The hydrogels may have been rehydrated due to the humidity at room temperature while transferring it to the CPD technique. In the CPD technique, ethanol will only exchange efficiently with liquid carbon dioxide. A partly rehydrated hydrogel will thus be more susceptible to a collapse. For hydrogels with GNRs, there are fewer collapse characteristics. The GNR-hydrogel exhibits rather a highly entropic polymer network. The GNRs may have reinforced the polymer network making it less susceptible to a collapse during the CPD. The complexity of the GNR reinforced polymer network could be due to the hydrophilicity of the AAM-AAC-BIS hydrogels. The anionic AAC co-monomer may contribute to absorb a more substantial

Preprints (www.preprints.org) | NOT PEER-REVIEWED | Posted: 26 April 2018 doi:10.20944/preprints201804.0335.v1

fraction of water in the small pores of the polymer network. The preparation methods may also influence the pore structures as discussed in Section 2.3 [48,49].

Figure 5c and 5d shows HMDS dried hydrogels without and with GNRs in BSE mode, respectively. HMDS dried hydrogel without GNRs shows less collapsed network than the CPD hydrogel without GNRs. This might indicate that the hydrogel is less susceptible to rehydration by using drying in HMDS solvent than using the CPD technique. For HMDS dried hydrogel with GNRs, the polymer network is highly entropic with few collapsing features. These observations coincide with the observations made in Figure 5a and 5b, where the GNRs is assumed to reinforce the polymer network making it less susceptible to collapse during the drying. The complexity of the GNR reinforced polymer network may also be due to the hydrophilicity of the AAM-AAC-BIS anionic hydrogel.

As for the results obtained in Section 2.1 there are high contrast features along the edges of the polymer networks in Figure 5d in BSE mode (indicated with white arrows), which could represent dense materials. The high contrast features are however similar for hydrogel, with and without GNRs, and makes the quantizing of the distribution of GNRs in the polymer network uncertain. The sizes and shapes of the contrast features could be a result of the artifacts introduced from the sample preparations [63,64].

Figure 6 shows SEM images of CPD and HMDS dried hydrogels with GNRs at a higher magnification than the SEM images in Figure 5. SEM image of GNR solution dried on carbon tape in Figure 6b is presented as a reference sample and used for comparison to the small-sized high contrast features observable in Figure 6a and 6c shown with white arrows.

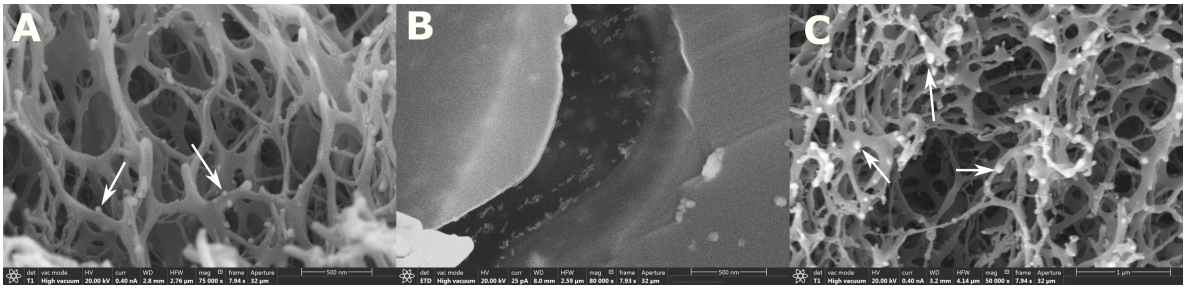

Figure 6. (**a**) SEM image of CPD AAM-AAC-BIS hydrogel with GNRs in BSE mode; (**b**) Air-dried GNR solution on carbon tape in SE mode for comparison with SEM images of GNP-hydrogels; (**c**) SEM image of HMDS dried AAM-AAC-BIS hydrogel with GNP in BSE mode. The white arrows clarifies the small-sized high contrast features observed that could indicate distributed GNRs.

The branched and highly entropic polymer networks of AAM-AAC-BIS GNR-hydrogels can be qualitatively assessed in Figure 6a and 6c. The pore size and shapes are more irregular for AAM-AAC-BIS GNR-hydrogels as compared to the AAM-BIS hydrogels. The irregular pore size and shapes of AAM-AAC-BIS GNR-hydrogels could be due to the hydrophilic nature of the anionic polymer network as discussed for Figure 5b and 5d.

The small-contrast features in Figure 6a and 6c (shown with white arrows) are similar results to those in Figure 4a and 4c which could indicate the presence of GNRs since they are denser than the polymer network. As discussed for the results in Figure 4, these small-sized contrast features are difficult to quantize as a distribution of GNRs due to the low contrast intensity, but could be improved by using results from [65,66].

2.3. Influence of Fixation, Dehydration and Drying on the Morphological Structures of the GNR-Hydrogel

The AAM-BIS hydrogel is sensitive towards ethanol concentrations but insensitive to pH for the solutions used in this paper [67]. The fixation with glutaraldehyde at pH 7.2 will therefore introduce small changes in the hydrogel swelling equilibrium with respect to changes in pore size and shapes. However, for the dehydration with ethanol, the hydrogel will decrease in size, which can be assumed

to result in considerable changes in size and shape of pores of the polymer network. The pore sizes observed in Figure 3 and 4 are thus assumed to be smaller than the pore size of the hydrogel in a hydrated state. The dried hydrogels may also in most cases exhibit an uncertain degree of collapsing characteristics [48,49,54,55,68]. Thus, any degree of collapsing characteristics of the hydrogel may result in a close packing of the GNRs. The amount of close-packed GNRs in the BSE mode SEM images were however difficult to characterize in our results due to the low contrast of GNRs. Other microscopy tecniques may be used to study its native hydrated state such as by using cryogenic or environmental SEM that omits the fixation, dehydration and the drying [51,56].

The AAM-AAC-BIS hydrogel is sensitive to both ethanol and pH [67,69]. The fixation with glutaraldehyde at pH 7.2 causes the hydrogel to swell significantly due to the deprotonation of the AAC making the polymer network highly anionic. This may pose strain on the polymer network beyond the elastic limit. Hence, the irregular shapes of the polymer network in Figure 5b and 5d can be caused by the swelling of the hydrogel. The dehydration of the hydrogel with ethanol causes the hydrogel to contract significantly. The pore size observed in Figure 5 and 6 is thus assumed to be smaller than the pore size of the hydrogel in its native hydrated state. As mentioned above, it is possible to study hydrogels in its native hydrated state by using cryogenic or environmental SEM [51,56], to reduce any degree of hydrogel collapse [48,49,54,55,68] that may result in a close packing of GNRs.

3. Conclusions

The morphology of low weight percentage polyacrylamide and poly(acrylamide-co-acrylic acid) hydrogels, with and without GNRs, have been characterized by using conventional SEM. A comparison was made between the CPD and HMDS drying methods of hydrogels. Results from CPD and HMDS techniques shows to have comparable pore structures. Hence, using HMDS solvent for drying may serve as a suitable alternative to the CPD technique. The HMDS technique is a cost-effective substitution of the CPD technique that omits equipment use as well as it less time consuming. The pores of poly(acrylamide-co-acrylic acid) hydrogels shows to have irregular structures while the pores of polyacrylamide hydrogels shows to have more regular structures. This difference is assumed to be due to the more substantial hydrophilicity of poly(acrylamide-co-acrylic acid) anionic hydrogel. The pore structures of the dehydrated and dried hydrogels can be assumed to be smaller than the pore structures of hydrated hydrogels due to the water exchange with ethanol in the dehydration. The effect of dehydrating and drying hydrogels may in most cases exhibit an uncertain degree of collapsing characteristics [48,49,54,55,68]. By comparing the morphology of dried hydrogels with cryoSEM or environmental SEM images of hydrated hydrogels [51,56] it is possible to estimate the presence of these collapsing features.

Small-sized high contrast features can be observed from the BSE mode SEM images of GNR-hydrogels, which may indicate the presence of GNRs since they are denser than the polymer network. The contrast of these features were however not significant enough for distinguishing them from artifacts associated to the sample preparations [63,64]. The contrast of NMNPs in gel-like samples may be improved by omitting the sample coating and by instead including highly conductive sample holders [65], or by using both SE and BSE detectors to obtain density dependent contrasts that highlights the high densities areas in the image [66]. Any hydrogel collapse may result in close packing of the GNRs. The amount of close-packed GNRs in the BSE mode SEM images were however difficult to characterize in our results due to the low contrast of the GNRs.

Future work will consist of developing methods for enhancing the contrast of high-density materials in a low-density matrix for conventional SEM imaging. Furthermore, volume-imaging methods such as the FIB-SEM or the SBFSEM techniques will be used to map the distribution of metal nanoparticles in hydrogels.

 doi:10.20944/preprints201804.0335.v1

4. Experimental Section

4.1. Materials for synthesizing hydrogels

The materials used for synthesizing hydrogels, with and without GNPs, are as follows; acrylamide (AAM) (99%, Sigma Aldrich, Schnelldorf, Germany), acrylic acid (AAC) (99%, Sigma Aldrich), *N*,*N*-methylenebisacrylamide (BIS) (≥99.5%, Sigma Aldrich), 1-hydroxycyclohexyl phenyl ketone (99%, Sigma Aldrich), dimethyl sulfoxide (DMSO) (≥99.9%, Sigma Aldrich), citrate-stabilized 670 nm-resonant GNRs (50 nm in length, 19 nm in diameter, 1.14×10^{13} particles/mL, 2 mM citrate buffer, nanoCompix), phosphate-buffered saline (PBS) (Tablet, Sigma Aldrich), squalane (99%, Sigma Aldrich) and milli-Q (mQ) water (resistivity 18.2 M/cm, Millipore Simplicity 185), pentane (Van Water & Rogers, VWR, Radnor, PA, USA).

4.2. Synthesizing Bulk Volume of Hydrogel With and Without Gold Nanoparticles

Two stock solutions were prepared and used later for making pre-gel samples. First stock solution was prepared by dissolving AAM and BIS in PBS solution (30 wt% AAM-BIS and 2 mol% BIS). Second stock solution was prepared by dissolving AAM, AAC, and BIS in PBS solution (30 wt% AAM-AAC-BIS, 2 mol% BIS, molar ratio AAM/AAC = 1/2). The stock solutions were stored at 4 °C until further use for up to two weeks. 10 wt% AAM-BIS and 10 wt% AAM-AAC-BIS pre-gel samples were further prepared by diluting the stock solutions with PBS or GNP solution. Thus, four types of pre-gel samples where made; (1) 10 wt% AAM-BIS in PBS solution; (2) 10 wt% AAM-BIS in GNP solution; (3) 10 wt% AAM-AAC-BIS in PBS solution; (4) 10 wt% AAM-AAC-BIS in GNP solution. The pre-gel samples were stored at 4 °C until further use for up to 24 hours. Next, 1-hydroxycyclohexyl phenyl ketone photoinitiator (PI) was diluted in DMSO (0.01 M). Before photopolymerization, the PI-DMSO solution was added to the pre-gel sample (PI/pre-gel = 31/2000). 0.2 mL pre-gel with PI solution was further transferred by a pipette (Finpippette F2, Thermo Scientific, VWR) to a glass rod surrounded by 1.3 mL squalane-PI oil (2.7 mg/mL PI) in a 1.5 mL eddendorf tube (211-2164, VWR) as shown in Figure 7.

Figure 7. Image of eppendorf tube with glass rod inside used for photopolymerizing pre-gel in squalane-PI.

The deposited pre-gel with PI solution on glass rod forms a hemispherical shape since it is immiscible in the squalane-PI oil. The hemispherical pre-gel with PI on the glass rod was illuminated with light at 365 nm by using a Ø400 μm multimode OF (QP400-2-UV-VIS, Ocean Optics, Dunedin, FL, USA) coupled to a LED (M365F1, Thorlabs, Newton, NJ, USA). The pre-gel with PI was

 doi:10.20944/preprints201804.0335.v1

photopolymerized for 15 minutes, subsequently transfered to pentane to remove impurities for 5 s and stored in PBS solution (pH of PBS adjusted to 4.5 for AAM-AAC-BIS hydrogel) until further use.

4.3. Preparing Hydrogels for Scanning Electron Microscopy

The materials used for preparing hydrogles for SEM are as follows; 2.5% glutaraldehyde (Chemi-Teknik AS, Oslo, Norway) in Sorensens phophate buffer (SPBS) (pH 7.2), ethanol (absolute alcohol, Antibac AS, Oslo, Norway), and hexamethyldisilazane (HMDS) ($\geq$ 99%, Sigma-Aldrich).

The AAM-BIS and AAM-AAC-BIS hydrogels, with and without GNP, were fixated in 2.5 % glutaraldehyde (Chemi-Teknik AS, Oslo, Norway) in SPBS (pH 7.2) for 2 hours at room temperature and left for 12 hours at 4 °C. After fixation, the hydrogels were washed two times for 5 minutes in SPBS. The pre-gel samples were further cut in half by a razor where one half was prepared for the critical point drying technique (CPD) (Polaron) and the other half was prepared for drying using HMDS solvent. Before drying, the hydrogels were dehydrated with increased ethanol concentrations of 10, 25, 50, 70, 90 and 100%, 5 minutes for each concentration. Further, one gel serie from the razor cutting was transferred to the CPD, while the other gel serie from the razor cutting was transferred to HMDS solvent. With the CPD technique, the ethanol was replaced with liquid carbon dioxide and further sublimed entirely. With HMDS solvent, the gel was transferred first to 50% HMDS diluted in ethanol for 20 min and then transferred to 100% HMDS. Two times for 20 min each round. The hydrogels in HMDS solvent were further dried overnight in a desiccator. The dried samples were cut or cracked in two by a razor, mounted on pins using double sided carbon tape, and sputter-coated (E5100, Polaron) with 30 nm of gold-palladium (Au/Pd). The samples were examined using a scanning electron microscope (Teneo Volumescope, Thermo Scientific Fisher), using Everhart-Thornley detector (ETD) in SE mode and Trinity detector (T1) in BSE mode.

4.4. Preparing GNPs on Carbon Tape for Scanning Electron Microscopy

An aliquot of GNP solution was transferred to double sided carbon tape, dried overnight in a desiccator and sputter coated with 30 nm gold-palladium (Au/Pd).

Acknowledgments: This work was supported by strategic research funding from Norwegian University of Science and Technology (NTNU). The work was also supported in part by the Interreg Sweden-Norway program (IR2015.01) and Energy and Sensor Systems (ENERSENSE, strategic research program at NTNU). The electron microscopy work was performed at EM laboratory, the Cellular and Molecular Imaging Core Facility (CMIC) at NTNU.

Author Contributions: Harald Ian Muri, Linh Hoang and Dag Roar Hjelme conceived and designed the experiments; Harald Ian Muri and Linh Hoang performed the experiments; Harald Ian Muri, Linh Hoang and Dag Roar Hjelme analyzed the data; Harald Ian Muri, Linh Hoang and Dag Roar Hjelme wrote the paper.

Conflicts of Interest: The authors declare no conflict of interest.

References

1. Todd R. Hoare a.; Daniel S. Kohane. Hydrogels in drug delivery: Progress and challenges. *Polymer* **2008**, *48*, 1993–2007.
2. RATNER, B.D.; HOFFMAN, A.S. Synthetic Hydrogels for Biomedical Applications. In *Hydrogels for Medical and Related Applications*; AMERICAN CHEMICAL SOCIETY, 1976; Vol. 31, *ACS Symposium Series*, p. 1.
3. Caló, E.; Khutoryanskiy, V.V. Biomedical applications of hydrogels: A review of patents and commercial products. *European Polymer Journal* **2015**, *65*, 252–267.
4. Xie, M.; Olderøy, M.Ø.; Andreassen, J.P.; Selbach, S.M.; Strand, B.L.; Sikorski, P. Alginate-controlled formation of nanoscale calcium carbonate and hydroxyapatite mineral phase within hydrogel networks. *Acta Biomaterialia* **2010**, *6*, 3665–3675.
5. Gawel, K.; Barriet, D.; Sletmoen, M.; Stokke, B.T. Responsive Hydrogels for Label-Free signal transduction within biosensors, 2010.
6. Lee, K.Y.; Mooney, D.J. Hydrogels for Tissue Engineering. *Chemical Reviews* **2001**, *101*, 1869–1880.

7. Holtz, J.H.; Asher, S.A. Polymerized colloidal crystal hydrogel films as intelligent chemical sensing materials. *Nature* **1997**, *389*, 829.
8. Alexeev, V.L.; Sharma, A.C.; Goponenko, A.V.; Das, S.; Lednev, I.K.; Wilcox, C.S.; Finegold, D.N.; Asher, S.A. High Ionic Strength Glucose-Sensing Photonic Crystal. *Analytical Chemistry* **2003**, *75*, 2316–2323.
9. Firestone, B.A.; Siegel, R.A. Dynamic pH-dependent swelling properties of a hydrophobic polyelectrolyte gel. *Polymer communications Guildford* **1988**, *29*, 204–208.
10. Brannon-Peppas, L. e Peppas, N. Dynamics and equilibrium swelling behaviour of pH-sensitive hydrogels containing 2-hydroxy methacrylate. *Biomaterials* **1990**, *11*, 635–644.
11. Deen, G.R.; Mah, C.H. Influence of external stimuli on the network properties of cationic poly(N-acryloyl-N'-propyl piperazine) hydrogels. *Polymer (United Kingdom)* **2016**, *89*, 55–68.
12. Kim, J.H.; Lee, S.B.; Kim, S.J.; Lee, Y.M. Rapid temperature/pH response of porous alginate-g-poly(N-isopropylacrylamide) hydrogels. *Polymer* **2002**, *43*, 7549–7558.
13. Lue, S.J.; Chen, C.H.; Shih, C.M. Tuning of Lower Critical Solution Temperature (LCST) of Poly(N-Isopropylacrylamide-co-Acrylic acid) Hydrogels. *Journal of Macromolecular Science, Part B* **2011**, *50*, 563–579.
14. Tanaka, T. Collapse of gels and the critical endpoint. *Physical Review Letters* **1978**, *40*, 820–823.
15. Rička, J.; Tanaka, T. Swelling of Ionic Gels: Quantitative Performance of the Donnan Theory. *Macromolecules* **1984**, *17*, 2916–2921.
16. Park, T.G.; Hoffman, A.S. Sodium Chloride-Induced Phase Transition in Nonionic Poly(N-isopropylacrylamide) Gel. *Macromolecules* **1993**, *26*, 5045–5048.
17. Brannon-Peppas, L.; Peppas, N.A. Time-Dependent Response of Ionic Polymer Networks to Ph and Ionic-Strength Changes. *International Journal of Pharmaceutics* **1991**, *70*, 53–57.
18. Miyata, T.; Asami, N.; Uragami, T. A reversibly antigen-responsive hydrogel. *Nature* **1999**, *399*, 766.
19. Takashi, M.; Asami, N.; Uragami, T. Structural design of stimuli-responsive bioconjugated hydrogels that respond to a target antigen. *Journal of Polymer Science, Part B: Polymer Physics* **2009**, *47*, 2144–2157, [arXiv:cond-mat/0406218].
20. Miyata, T.; Asami, N.; Uragami, T. Preparation of an antigen-sensitive hydrogel using antigen-antibody bindings. *Macromolecules* **1999**, *32*, 2082–2084.
21. Miyata, T.; Jige, M.; Nakaminami, T.; Uragami, T. Tumor marker-responsive behavior of gels prepared by biomolecular imprinting. *Proceedings of the National Academy of Sciences of the United States of America* **2006**, *103*, 1190–1193.
22. Tierney, S.; Falch, B.M.H.; Hjelme, D.R.; Stokke, B.T. Determination of Glucose Levels Using a Functionalized Hydrogel Optical Fiber Biosensor: Toward Continuous Monitoring of Blood Glucose in Vivo. *Anal. Chem.* **2009**, *81*, 3630–3636.
23. Bjørnøy, S.H.; Bassett, D.C.; Ucar, S.; Andreassen, J.P.; Sikorski, P. Controlled mineralisation and recrystallisation of brushite within alginate hydrogels. *Biomedical Materials (Bristol)* **2016**, *11*, 15013.
24. Thomas, V.; Namdeo, M.; Murali Mohan, Y.; Bajpai, S.K.; Bajpai, M. Review on Polymer, Hydrogel and Microgel Metal Nanocomposites: A Facile Nanotechnological Approach. *Journal of Macromolecular Science, Part A* **2007**, *45*, 107–119.
25. Murali Mohan, Y.; Lee, K.; Premkumar, T.; Geckeler, K.E. Hydrogel networks as nanoreactors: A novel approach to silver nanoparticles for antibacterial applications. *Polymer* **2007**, *48*, 158–164.
26. Das, A.; Kumar, A.; Patil, N.B.; Viswanathan, C.; Ghosh, D. Preparation and characterization of silver nanoparticle loaded amorphous hydrogel of carboxymethylcellulose for infected wounds. *Carbohydrate Polymers* **2015**, *130*, 254–261.
27. Liang, D.; Lu, Z.; Yang, H.; Gao, J.; Chen, R. Novel Asymmetric Wettable AgNPs/Chitosan Wound Dressing: In Vitro and In Vivo Evaluation. *ACS Applied Materials & Interfaces* **2016**, *8*, 3958–3968.
28. Tokarev, I.; Tokareva, I.; Gopishetty, V.; Katz, E.; Minko, S. Specific Biochemical-to-Optical Signal Transduction by Responsive Thin Hydrogel Films Loaded with Noble Metal Nanoparticles. *Advanced Materials* **2010**, *22*, 1412–1416.
29. Deen, R.G.; Chua, V. Synthesis and Properties of New "Stimuli" Responsive Nanocomposite Hydrogels Containing Silver Nanoparticles, 2015.
30. Mayer, K.M.; Hafner, J.H. Localized Surface Plasmon Resonance Sensors. *Chem. Rev.* **2011**, *111*, 3828–3857.

31. Maier, S.A. *Plasmonics: Fundamentals and applications*; Springer Science & Business Media, 2007; pp. 1–223, [arXiv:1011.1669v3].
32. Klimov, V. *Nanoplasmonics*; Pan Stanford Publishing, 2014.
33. Endo, T.; Kerman, K.; Nagatani, N.; Hiepa, H.M.; Kim, D.K.; Yonezawa, Y.; Nakano, K.; Tamiya, E. Multiple Label-Free Detection of Antigen-Antibody Reaction Using Localized Surface Plasmon Resonance-Based Core-Shell Structured Nanoparticle Layer Nanochip. *Analytical Chemistry* **2006**, *78*, 6465–6475.
34. Estevez, M.C.; Otte, M.A.; Sepulveda, B.; Lechuga, L.M. Trends and challenges of refractometric nanoplasmonic biosensors: A review. *Analytica Chimica Acta* **2014**, *806*, 55–73.
35. Gil, E.S.; Hudson, S.M. Stimuli-reponsive polymers and their bioconjugates. *Progress in polymer science* **2004**, *29*, 1173–1222.
36. Kelly, K.L.; Coronado, E.; Zhao, L.L.; Schatz, G.C. The optical properties of metal nanoparticles: The influence of size, shape, and dielectric environment. *Journal of Physical Chemistry B* **2003**, *107*, 668–677, [NIHMS150003].
37. Jain, P.K.; El-Sayed, M.A. Plasmonic coupling in noble metal nanostructures. *Chemical Physics Letters* **2010**, *487*, 153–164.
38. Jain, P.K.; Eustis, S.; El-Sayed, M.A. Plasmon Coupling in Nanorod Assemblies: Optical Absorption, Discrete Dipole Approximation Simulation, and Exciton-Coupling Model. *The Journal of Physical Chemistry B* **2006**, *110*, 18243–18253.
39. Jain, P.K.; Huang, W.; El-Sayed, M.A. On the universal scaling behavior of the distance decay of plasmon coupling in metal nanoparticle pairs: A plasmon ruler equation. *Nano Letters* **2007**, *7*, 2080–2088, [1106.1690].
40. Kreibig, U.; Volmerr, M. *Optical Properties of Metal Clusters*; Vol. 25, Springer Science & Business Media, 1995; p. 552, [arXiv:1011.1669v3].
41. Muri, H.I.; Hjelme, D.R. LSPR coupling and distribution of interparticle distances between nanoparticles in hydrogel on optical fiber end face. *Sensors (Switzerland)* **2017**, *17*, 2723.
42. Muri, H.I.D.I.H.; Bano, A.; Hjelme, D.R.D. A single point, multiparameter, fiber optic sensor based on a combination of interferometry and LSPR.
43. Muri, H.H.I.; Bano, A.; Hjelme, D.R.D. LSPR and Interferometric Sensor Modalities Combined Using a Double-Clad Optical Fiber. *Sensors* **2018**, *18*, 187.
44. Maier, S.A.; Brongersma, M.L.; Kik, P.G.; Atwater, H.A. Observation of near-field coupling in metal nanoparticle chains using far-field polarization spectroscopy. *Phys. Rev. B* **2002**, *65*, 193408—-.
45. Torquato, S.; Lu, B.; Rubinstein, J. Nearest-neighbor distribution functions in many-body systems. *Phys. Rev. A* **1990**, *41*, 2059–2075.
46. Lu, B.; Torquato, S. Nearest-surface distribution functions for polydispersed particle systems. *Phys. Rev. A* **1992**, *45*, 5530–5544.
47. Torquato, S.; Lee, S.B. Computer simulations of nearest-neighbor distribution functions and related quantities for hard-sphere systems. *Physica A: Statistical Mechanics and its Applications* **1990**, *167*, 361–383.
48. Lin, S.Y.; Chen, K.S.; Run-Chu, L. Drying methods affecting the particle sizes, phase transition, deswelling/reswelling processes and morphology of poly(N-isopropylacrylamide) microgel beads. *Polymer* **1999**, *40*, 6307–6312.
49. Rüchel, R.; Brager, M.D. Scanning electron microscopic observations of polyacrylamide gels. *Analytical Biochemistry* **1975**, *68*, 415–428.
50. Zhang, X.Z.; Yang, Y.Y.; Chung, T.S.; Ma, K.X. Preparation and Characterization of Fast Response Macroporous Poly(N-isopropylacrylamide) Hydrogels. *Langmuir* **2001**, *17*, 6094–6099.
51. Zhang, J.; Peppas, N.A. Morphology of poly(methacrylic acid)/poly(N-isopropyl acrylamide) interpenetrating polymeric networks. *Journal of Biomaterials Science, Polymer Edition* **2002**, *13*, 511–525.
52. Plieva, F.M.; Savina, I.N.; Deraz, S.; Andersson, J.; Galaev, I.Y.; Mattiasson, B. Characterization of supermacroporous monolithic polyacrylamide based matrices designed for chromatography of bioparticles. *Journal of Chromatography B* **2004**, *807*, 129–137.
53. Savina, I.N.; Mattiasson, B.; Galaev, I.Y. Graft polymerization of acrylic acid onto macroporous polyacrylamide gel (cryogel) initiated by potassium diperiodatocuprate. *Polymer* **2005**, *46*, 9596–9603.
54. Trieu, H.H.; Qutubuddin, S. Polyvinyl alcohol hydrogels I. Microscopic structure by freeze-etching and critical point drying techniques. *Colloid and Polymer Science* **1994**, *272*, 301–309.

55. Chen, J.; Park, K. Synthesis and characterization of superporous hydrogel composites. *Journal of Controlled Release* **2000**, *65*, 73–82.
56. Plieva, F.M.; Karlsson, M.; Aguilar, M.R.; Gomez, D.; Mikhalovsky, S.; Galaev', I.Y. Pore structure in supermacroporous polyacrylamide based cryogels. *Soft Matter* **2005**, *1*, 303–309.
57. Park, S.; Murthy, P.S.K.; Park, S.; Mohan, Y.M.; Koh, W.G. Preparation of silver nanoparticle-containing semi-interpenetrating network hydrogels composed of pluronic and poly(acrylamide) with antibacterial property. *Journal of Industrial and Engineering Chemistry* **2011**, *17*, 293–297.
58. Möbus, G.; Inkson, B.J. Nanoscale tomography in materials science. *Materials Today* **2007**, *10*, 18–25.
59. Kulawik, K.; Buffat, P.A.; Kruk, A.; Wusatowska-sarnek, A.M.; Czyrska-filemonowicz, A. Materials Characterization Imaging and characterization of γ' and γ'' nanoparticles in Inconel 718 by EDX elemental mapping and FIB - SEM tomography. *Materials Characterization* **2015**, *100*, 74–80.
60. Schneider, P.; Meier, M.; Wepf, R.; Müller, R. Serial FIB/SEM imaging for quantitative 3D assessment of the osteocyte lacuno-canalicular network. *Bone* **2018**, *49*, 304–311.
61. Jurrus, E.; Hardy, M.; Tasdizen, T.; Fletcher, P.T.; Koshevoy, P.; Chien, C.B.; Denk, W.; Whitaker, R. Axon tracking in serial block-face scanning electron microscopy. *Medical Image Analysis* **2018**, *13*, 180–188.
62. Denk, W.; Horstmann, H. Serial Block-Face Scanning Electron Microscopy to Reconstruct Three-Dimensional Tissue Nanostructure. *PLOS Biology* **2004**, *2*, e329.
63. Mehdizadeh Kashi, A.; Tahemanesh, K.; Chaichian, S.; Joghataei, M.T.; Moradi, F.; Tavangar, S.M.; Mousavi Najafabadi, A.S.; Lotfibakhshaiesh, N.; Pour Beyranvand, S.; Fazel Anvari-Yazdi, A.; Abed, S.M. How to Prepare Biological Samples and Live Tissues for Scanning Electron Microscopy (SEM). *Galen Medical Journal; Vol 3, No 2 (2014): June 2014* **2014**.
64. Little, B.; Wagner, P.; Ray, R.; Pope, R.; Scheetz, R. Biofilms: An ESEM evaluation of artifacts introduced during SEM preparation. *Journal of Industrial Microbiology* **1991**, *8*, 213–221.
65. GOLDSTEIN, A.; SOROKA, Y.; FRUŠIĆ-ZLOTKIN, M.; POPOV, I.; KOHEN, R. High resolution SEM imaging of gold nanoparticles in cells and tissues. *Journal of Microscopy* **2014**, *256*, 237–247.
66. Bertazzo, S.; Gentleman, E.; Cloyd, K.L.; Chester, A.H.; Yacoub, M.H.; Stevens, M.M. Nano-analytical electron microscopy reveals fundamental insights into human cardiovascular tissue calcification. *Nature Materials* **2013**, *12*, 576.
67. Bouchal, K.; Sedláková, Z.; Ilavský, M. Phase transition in swollen gels. *Polymer Bulletin* **1994**, *32*, 331–338.
68. Yeong, W.Y.; Chua, C.K.; Leong, K.F.; Chandrasekaran, M.; Lee, M.W. Comparison of drying methods in the fabrication of collagen scaffold via indirect rapid prototyping. *Journal of Biomedical Materials Research Part B: Applied Biomaterials* **2007**, *82B*, 260–266.
69. Shibayama, M.; Ikkai, F.; Inamoto, S.; Nomura, S.; Han, C.C. pH and salt concentration dependence of the microstructure of poly(N-isopropylacrylamide-co-acrylic acid) gels. *The Journal of Chemical Physics* **1996**, *105*, 4358–4366.